



Graphene Properties, Synthesis and Applications: A Review

AKANKSHA R. URADE,¹ INDRANIL LAHIRI,^{1,2} and K.S. SURESH ^{2,3}

1.—Centre of Excellence: Nanotechnology, Indian Institute of Technology Roorkee, Roorkee 247667, India. 2.—Department of Metallurgical and Materials Engineering, Indian Institute of Technology Roorkee, Roorkee 247667, India. 3.—e-mail: ks.suresh@mt.iitr.ac.in

We have evaluated some of the most recent breakthroughs in the synthesis and applications of graphene and graphene-based nanomaterials. This review includes three major categories. The first section consists of an overview of the structure and properties, including thermal, optical, and electrical transport. Recent developments in the synthesis techniques are elaborated in the second section. A number of top-down strategies for the synthesis of graphene, including exfoliation and chemical reduction of graphene oxide, are discussed. A few bottom-up synthesis methods for graphene are also covered, including thermal chemical vapor deposition, plasma-enhanced chemical vapor deposition, thermal decomposition of silicon, unzipping of carbon nanotubes, and others. The final section provides the recent innovations in graphene applications and the commercial availability of graphene-based devices.

INTRODUCTION

In 2004, Geim et al. synthesized a stable monolayer of graphene through mechanical stripping. Geim and Novoselov were awarded the Nobel Prize in Physics in 2010 for their successful experiments, and, subsequently, graphene became one of the world's most studied two-dimensional materials.¹ Graphene is a single atomic layer of carbon atoms arranged in a hexagonal pattern. It has a thickness of only 0.334 nm, making it the world's thinnest material. It has numerous distinguishing qualities due to its unique properties, such as a large specific surface area ($\sim 2600 \text{ m}^2/\text{g}$),¹ high electron mobility ($200,000 \text{ cm}^2/\text{Vs}$),² enhanced thermal conductivity ($3000\text{--}5000 \text{ Wm/K}$),³ extreme optical transparency (97.4%),⁴ and exceptional mechanical strength, with a Young's modulus of 1 TPa.⁵

An experimental demonstration of the thermal chemical vapor deposition (CVD) method for synthesizing a few-layer nano-graphene with roughly 35 layers of graphene was made 2 years after the first report on graphene synthesis.⁶ To create a large-area graphitic film with three to six graphene layers, Obraztsov et al. resorted to the CVD

approach.⁷ Eda et al. produced large-area (10 cm^2) reduced graphene oxide (rGO) film using the vacuum infiltration method.⁸ In 2009, Li et al. used the CVD approach to successfully create high-quality, large-area uniform graphene sheets on copper substrates.⁹ In their study, more than 95% of the 1-cm^2 film was monolayer graphene, 3–4% was bilayer graphene (BLG), and the remaining 1% was few-layer graphene (FLG). They discovered that graphene formed on copper via a surface-catalyzed mechanism. They also demonstrated graphene synthesis on a quartz substrate with an improved approach for transferring graphene to other substrates with minimum defects. Bae et al. reported the first roll-to-roll (R2R) method for producing large-area 30-inch (c. 760 mm) diagonal films utilizing CVD on flexible ultra-large copper substrates.¹⁰ With the R2R approach, the films can be transferred directly onto the desired substrate. Paton et al. synthesized graphene nanoplatelets (GNP) from graphite by liquid phase exfoliations (LPE) in 2014.¹¹ The GNPs produced by LPE have a limited lateral dimension of a few micrometers, and can range in thickness from monolayer to more than ten layers. Later, Luong et al. established flash Joule heating as a quick, effective, and scalable method to produce graphene in a few grams from a range of feedstocks, including waste food, plastics, coal, carbon black, and petroleum coke.¹² This was

(Received May 28, 2022; accepted August 29, 2022; published online October 14, 2022)

the breakthrough research in the direction of graphene commercialization. The technique employs a “flash” of electricity to heat the carbon to approximately 3000 K, converting it into graphene flakes.

Graphene’s high electron mobility makes it an ideal material for semiconductor device applications requiring fast response times.^{13,14} The high conductivity of graphene combined with high optical transparency has attracted applications such as a transparent conductive layer for photonic devices.¹⁵ In addition to these, graphene holds a great deal of promise for other areas, such as anticorrosion coatings¹⁶ and paints,¹⁷ sensors,¹⁷ wearable and flexible displays,¹⁸ solar panels,¹⁹ faster DNA sequencing,²⁰ drug delivery,²¹ etc. Most of these applications require high-quality SLG or BLG. The last few years have seen much progress in the controllable synthesis and large-scale synthesis of graphene by mechanical exfoliation²² or chemical exfoliation,²³ as well as CVD.^{24,25} The production methods and subsequent processing techniques mostly decide the morphology and structure of the graphene, and also govern the potential applications. Therefore, Sect. 2 reports on the structure and properties, while Sect. 3 covers synthesis techniques, followed by a detailed discussion of its potential applications.

STRUCTURE AND PROPERTIES OF GRAPHENE

The number of layers of graphene regulates the different properties. SLG and BLG are zero band gap semiconductors owing to the encounter of the conduction and the valance bands at the Dirac points.²⁶ A band gap can be opened in BLG by the application of an electric field.²⁷ Furthermore, for FLG, the structure becomes more metallic with increasing layers.²⁸ Hence, to comprehend the application of graphene, it is crucial to first understand the graphene properties. This section will review the structure and properties of graphene.

Structure of Graphene

SLG is a sp^2 hybridized structure with two carbon atoms in a unit cell, and these two carbon atoms are located in the A and B positions, respectively (Fig. 1a).²⁹ BLG can be divided primarily into three categories: AA-stacked, AB-stacked, and twisted^{29,30} (Fig. 1b). On the other hand, tri-layer graphene (TLG) has three stacking options. The AAA, ABA, and ABC stacking sequences represent the hexagonal, Bernal, and rhombohedral arrangements, respectively³¹ (Fig. 1c). Three out of four valence electrons for each carbon atom in graphene’s honeycomb lattice overlap with the adjacent carbon atom within the sheet, forming a strong sigma bond. The exceptional flexibility and robustness of graphene’s lattice structure are due to the sigma bond. The remaining fourth electron in the Pz

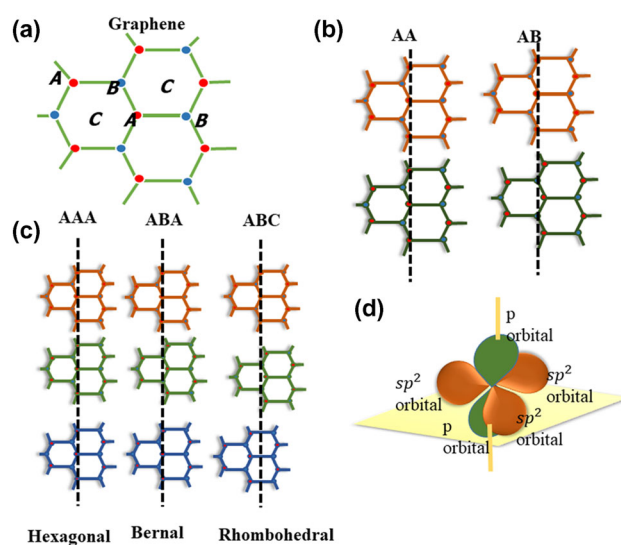


Fig. 1. (a) SLG structure, A and B denote carbon sites, (b) BLG stacking types, (c) TLG stacking types, (d) π bond and sigma bond positions in the graphene honeycomb lattice.

orbital overlaps with the neighboring orbitals and forms a π bond that regulates the interaction between the graphene layers (Fig. 1d).

Properties of Graphene

Two linear bands in the band structure of the SLG cross at the Fermi level in the first Brillouin zone, which are Dirac points. Graphene is thus a zero-gap semiconductor (Fig. 2a).²⁷ Holes and electrons near the Dirac point behave as massless fermions ($m^* = 0$) and travel at extremely high speeds (10^6 m/s). SLG is recognized as a crucial material for electronics devices due to its outstanding properties and high flexibility. However, the zero-gap constrains its applications. Hence, the first obstacle to overcome is the opening of a gap. A perpendicular electric field applied across the graphene layer tunes the band gap of BLG and TLG due to different stacking sequences.^{30,31} Oostinga et al. demonstrated the change in carrier mobility from $\sim 1,000$ cm^2/Vs to $\sim 3,000$ cm^2/Vs by tuning the gate voltage²⁷ (Fig. 2b–c).

In the low-energy region, Bernal TLG has two parabolic bands and one pair of linear bands, as shown in Fig. 2d.³² When the electric field exceeds 1 V/nm, the top of the valence band exceeds the bottom of the conduction band, and the band gap disappears. The energy gap of Bernal BLG varies monotonically with the electric field. Thus, Bernal TLG behaves like a semimetal in the perpendicular electric field. Near the K point, there are three pairs of parabolic bands for the rhombohedral TLG. When the perpendicular electric field is continuously increased, the energy gap for initially increases and then decreases. Bernal and rhombohedral TLG have different electronic properties due to stacking sequences.

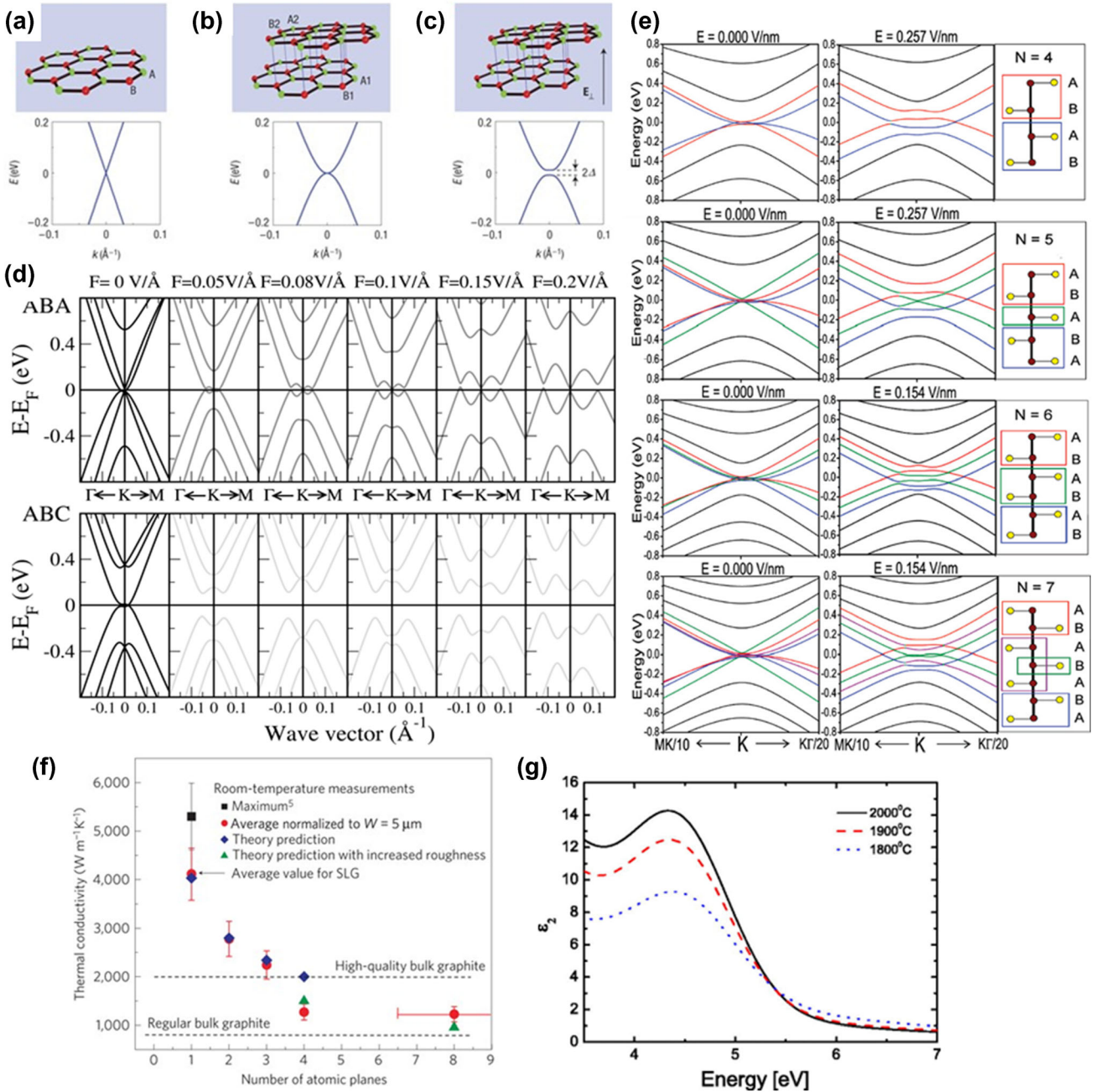


Fig. 2. Band structure of (a) SLG, (b) BLG without an electric field, and (c) BLG with perpendicular electric field (reprinted with permission from Ref. 27), (d) ABA and ABC stacked TLGs under an electric field (reprinted with permission from Ref. 32), (e) band structure of ABAB stacked FLGs under an electric field (reprinted with permission from Ref. 33), (f) thermal conductivity of FLG observed as a function of the number of atomic planes (reprinted with permission from Ref. 34), (g) imaginary part of graphene's dielectric function as it has evolved at various growth temperatures (reprinted with permission from Ref. 35).

FLG's electronic structure is extremely sensitive to thickness, becoming increasingly metallic with increasing layers. Tang et al. investigated the effects of an electric field on FLG with layer numbers greater than 4.³³ An external electric field can convert all ABC stacking graphene with $N > 4$ to semiconductors, whereas ABA stacking graphene remains semi-metallic (Fig. 2e).

In addition to its distinctive electrical properties, graphene has a very high thermal conductivity. At

ambient temperature, the intrinsic thermal conductivity of single-layer suspended graphene is in the range of 4800–5300 W/mK⁴. In comparison, high-quality graphite has a thermal conductivity of only 2000 W/mK. Suspended graphene from CVD has a thermal conductivity that ranges from 1500 to 5000 W/mK at room temperature (RT).³⁶ A number of independent experimental reports have validated graphene's high thermal conductivity values.^{37–40} The thermal conductivity of supported graphene at

RT is 600 W/mK and is lower than that of suspended graphene due to phonon scattering at the defects site and thermal coupling to the substrate.⁴¹ Graphene flake thermal conductivity changes with size, and that heat is transferred mainly by acoustic phonons. For instance, the thermal conductivity of suspended FLG initially reduces with an increasing number of layers, then recovers and reaches the bulk graphite limit of 2000 W/mK (Fig. 2f).³⁴ The intrinsic features defined by phonon–phonon scattering help to address the interdependence of thermal conductivities on the number of graphene layers. As the number of graphene layers increases, the phonon dispersion changes, resulting in more phonon states available for Umklapp scattering. The greater the Umklapp scattering, the lower the inherent thermal conductivity.

Graphene's unique optical feature can be attributed to its distinctive two-dimensional band structure.⁴² It has been shown from the linear optical characterization that graphene absorbs approximately 2.3% of the incident red light and 2.6% of the green light.⁴³ However, the relationship is linear, and each layer absorbs 2.3% of light. This means that a graphene sample with 5 layers would absorb 11.5% of light and be about 88% transparent.⁴⁴ In addition, graphene absorbs over a wide spectral range, from the visible to the infrared region.⁴⁵ Interband transitions could explain the light absorption from the visible to the near-infrared range. On the other hand, intraband transitions or free carrier absorption are responsible for the optical response in the far infrared range. As graphene lacks definite energy band levels, it can absorb the radiation regardless of its frequency. Graphene may also produce optical transitions in electric fields, known as gate-dependent optical transitions.⁴⁶ The low density of states at the Dirac point causes the Fermi level of graphene to change in the presence of an applied electrical field. This property is useful in electronics to modulate the current, because a change in the Fermi level modifies conductivity, as well as tunes the transmission of an optical source. Ni et al. obtained the refractive index (n) of monolayer graphene grown on a 285-nm-thick Si substrate as $n = 2.0 - 1.1i$ in the visible spectrum, slightly different from that of bulk graphite, $n_G = 2.6 - 1.3i$.⁴⁷ The refractive index of graphene on such substrates depends on the wavelength and the incident angle of the illumination. By fitting to experimental spectra as a function of wavelength, the complex refractive index of graphene and graphite may be generally represented as $n = 3 - iC/(3\lambda)$ (where λ is wavelength and $C = 5.446 \mu\text{m}^{-1}$).⁴⁸ Ochoa-Martínez et al. reported the refractive index of monolayer graphene as ~ 4 and for bilayer graphene as ~ 3.5 .⁴⁹ A dielectric function is the sum of real and imaginary dielectric functions.⁵⁰ The graph between imaginary dielectric function and critical point (CP) transition energy is used to deduce the thickness dependence of the

graphene on dielectric function. Bouhafs et al. reported that the dielectric function of graphene increases as the number of graphene layers grows, or as the temperature of graphene growth increases (Fig. 2g).³⁵ While graphene synthesized at 2000°C exhibits a dielectric function comparable to that of graphite, graphene formed at 1800°C exhibits graphene-like characteristics. The CP transition energy in the dielectric function of graphene is red-shifted with increasing thickness (or temperature), which is accompanied by an increase in polarizability, as shown in Fig. 2. Exceptionally higher mechanical properties of graphene have been assessed using an atomic force microscope, and the intrinsic breaking strength and elasticity of free-standing monolayer graphene are reported as 130 GPa and 1 TPa, respectively.^{51,52} Table I shows the comparison between some properties of SLG, BLG, FLG, GO, and rGO.

RECENT ADVANCES IN GRAPHENE SYNTHESIS TECHNIQUES

Ruoff et al.⁷⁵ separated the graphene layer from the graphite flakes using adhesive tape. Following exfoliation, these layers were dry-deposited on a silicon wafer, referred to as the 'Scotch tape' method. Later, Novoselov and co-workers successfully synthesized a high-quality monolayer graphene by the Scotch tape method.⁷⁶ Achieving high-quality graphene on a mass scale is one of the limiting issues to realizing its wide applications. The graphene synthesis techniques have been broadly classified in the following sections.

Exfoliation of Graphite

Even though the quality of graphene produced by Scotch tape or micromechanical cleavage is excellent,^{76,77} the yield is low, and the process is time-consuming. As a result, this method is limited to laboratory research and appears impractical for industrial production.⁷⁸ To improve the efficiency, Jayasena et al. reported a different mechanical cleavage approach for producing FLG from bulk graphite.⁷⁹ The technique exfoliates graphite with an ultra-sharp single-crystal diamond wedge, followed by ultrasonic oscillations. Narayan et al. obtained about 30% yield of SLG and FLG sheets with only a few defects by directly sonicating graphite flakes in an aromatic semiconducting surfactant perylene tetracarboxylate (PTCA).⁸⁰ They also observed that dried graphene/PTCA powders are easily re-dispersible in water.

Kaplan's group used silk nanofibers as a surfactant during shear mixing in a kitchen blender.⁸¹ They achieved graphene dispersion with > 30% yield of FLG with a production rate greater than 6 g/h. Xu et al. achieved production rates of up to 25 g/h for FLG (70% of that being 1–3 layers), with high conductivity and very low defect density, using electrochemically-assisted exfoliation.⁸² Keshri

et al. reported chemical- and solvent-free graphite exfoliation using plasma spraying. Most notably, without using a solvent, synthesis rates of up to 48 g/h have been documented, and a material cost of US\$1.12 g⁻¹ has been predicted with batch-to-batch repeatability⁸³ (Fig. 3).

Chemical Oxidation and Reduction Method

One of the traditional techniques for producing large amounts of graphene is the chemical reduction of GO. Initially, GO is produced via graphite oxidation using the modified Hummers method.⁸⁴ Then, the prepared GO is reduced by hydrazine⁸⁵ and sodium borohydride.⁸⁶ The chemical reducing agents like hydrazine are not environmentally friendly and create hazardous by-products.⁸⁷ Hence, researchers started to find safe and environmentally friendly reducing agents.⁸⁸

Abdolhosseinzadeh et al. reported fully scalable graphene mass production by reducing graphite oxide with ascorbic acid.⁸⁹ A different approach is with plant-based extracts being used as a reducing agent, as these are non-hazardous, comparatively cheap, and easily available in the market. Upadhyay et al. used grape extract as an alternative to the conventional toxic reducing agents.⁹⁰ Mahata et al. have used Tulsi leaf as a green alternative for bio-reduction of GO with 90% yield.⁹¹ In a recent review, Park et al. reported detailed information about the chemical methods for graphene production.⁹²

Thermal Chemical Vapor Deposition (CVD)

In the CVD method, gas species are brought into the reactor, where they travel through the hot zone. At the surface of the metal substrate, hydrocarbon

Table I. Comparison between some properties of SLG, BLG, FLG, GO, and rGO

Properties	SLG	BLG	FLG	GO	rGO
Surface area (m ² /g)	2630 ¹	1314 ⁵³	270–1500 ⁵⁴	736–2418 ^{55,56}	700 ⁵⁷
Optical transparency (%)	97.7 ⁴³	~ 95 ⁵⁸	84 ⁵⁹	70 ⁶⁰	80 ⁶⁰
Electron mobility (cm ² /Vs)	200,000 ⁶¹	~ 1 × 10 ^{5,62}	300–1150 ⁶³	200 ⁶⁴	320 ⁵⁹
Thermal conductivity (W/mK)	5000 ⁴	1900 ⁶⁵	1100 ⁶⁶	72–670 ⁶⁷	2275 ⁶⁸
Young's modulus (GPa)	1000 ⁵²	2000 ± 500 ⁶⁹	1850 ⁵⁹	32 ⁷⁰	250 ± 150 ⁷¹
Tensile strength	130 GPa ⁵²	94.9–300 GPa ⁷²	~ 200 GPa ⁷³	~ 120–263 MPa ^{70,74}	360 MPa ⁷⁴

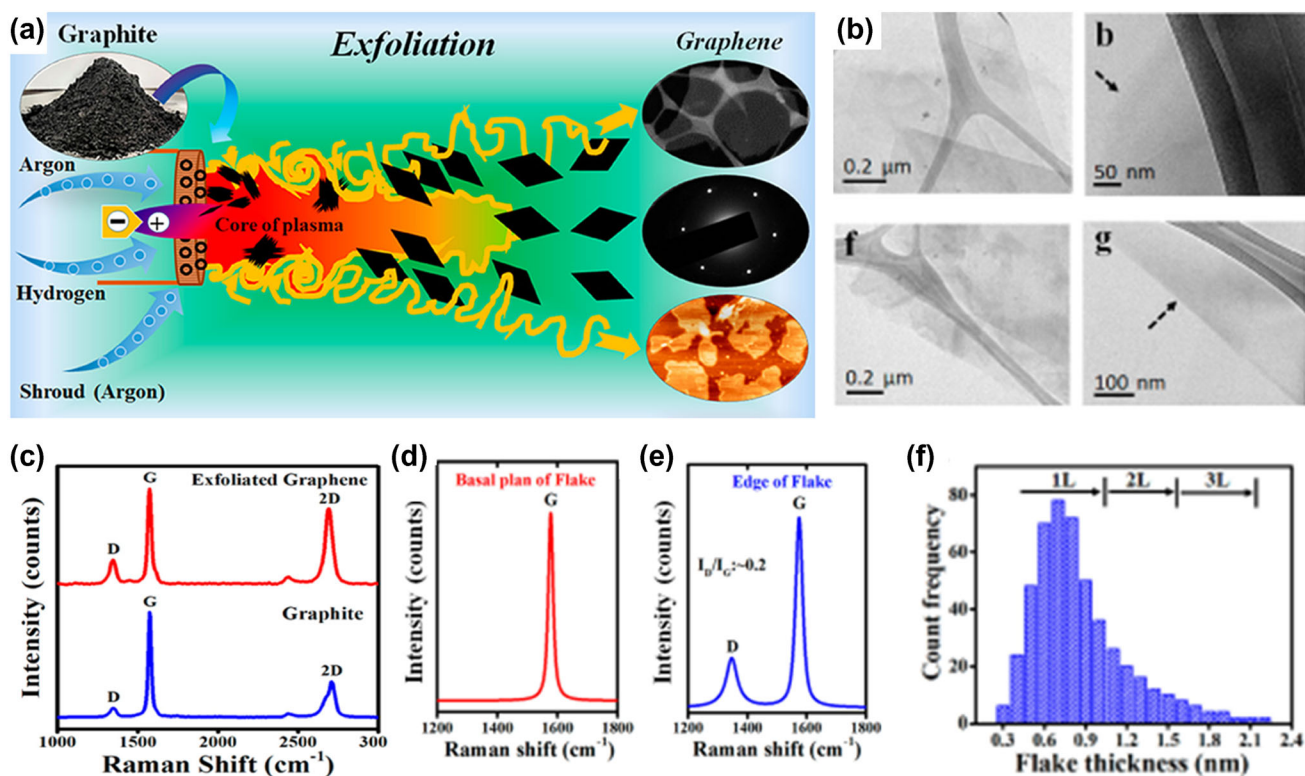


Fig. 3. (a) Graphite plasma spray exfoliation, (b) TEM images of SLG and BLG, (c–e) Raman spectra of the synthesized graphene, the basal plane and the edge of graphene flakes, (f) distribution of the thickness of graphene flakes (reprinted with permission from Ref. 83).

precursors break down into carbon radicals. These carbon radicals then self-assemble to form the graphene layer. In the course of the reaction, the metal substrate acts as a catalyst and affects the quality of graphene. In recent years, a variety of transition metals, such as Ru,⁹³ Ir,⁹⁴ Pt,^{95,96} Co,⁹⁷ Pd,⁹⁸ Ni,⁹⁹ and Cu,^{100–102} have been used as a catalyst.

The solubility of carbon in Cu is 0.04% at 1000°C.¹⁰³ The graphene growth happens via surface adsorption in Cu due to low solubility, while surface segregation/precipitation is the main mechanism in metals such as Ni having higher solubility. Therefore, it is easier to obtain a monolayer graphene on a Cu substrate. Wood et al. reported growing mono- to few-layer graphene on polycrystalline Cu at 1000°C using methane (CH₄). The crystal quality and the orientation of the Cu substrate greatly influenced the quality of the graphene growth. After CVD, Raman spectroscopy shows that the (111) having facets produce pristine monolayer graphene while Cu (100) surface prefers multilayer graphene growth. Epitaxial growth of large-area graphene on a (111)-oriented Cu single crystal is possible via CVD.¹⁰² Ishihara et al. reported the synthesis of SLG on Cu (111), and found that the Cu(111) is the optimal surface for defect-free graphene growth.¹⁰¹

The solubility of carbon in Ni is 2.03% at 1000°C and decreases with temperature. Since the formation of graphene on Ni is carbon segregation and precipitation, different cooling rates produce distinct segregation behaviors, affecting the thickness and the quality of the graphene films.¹⁰⁴ The atomically smooth surface in the single-crystal substrate enabled the preferential growth of monolayer/bilayer graphene, while, in a polycrystalline Ni substrate, multilayers were obtained.¹⁰⁵

Some of the major defects include wrinkles, folds, vacancies, line defects, adatoms, and impurities, all of which degrade graphene's performance for efficient applications. To overcome this issue, Ruoff et al. reported the synthesis of fold-free single-crystal graphene film on Cu-Ni(111) with dimensions of 4 cm × 7 cm¹⁰⁶ (Fig. 4a, b). Bae et al. reported CVD growth of monolayer graphene on large flexible Cu foils with dimensions as large as 30 inches (c. 760 mm) diagonally, which was then transferred to the target using the R2R method.¹⁰⁷ The graphene sheet resistance was as low as ~ 125 Ω/sq with 97.4% optical transmittance.

Plasma Chemical Vapor Deposition

The approaches to growing high-quality graphene films on transition metal substrates are dominated by high-temperature thermal CVD. A low-temperature process for graphene synthesis would be required for applications in electronic devices, and plasma CVD could be an excellent alternative to thermal CVD. The formation of plasma from the

reacting gas precursors enables thermal CVD deposition at a lower temperature.¹⁰⁹ Kim et al. decreased the synthesis temperature to 450 °C and reported graphene on Ni foil with the high transparency of 89%.¹¹⁰ Yamada et al. used microwave plasma CVD to create 294-mm-wide FLG films on a Cu substrate at 400°C with 95% optical transmittance (Fig. 4c, d).¹⁰⁸ With the lowest synthesis temperature of 317°C, graphene layers having optical transmittance in the range 78–94% have been achieved.¹¹¹

Thermal Decomposition of Silicon Carbide (SiC)

Although the CVD technique has emerged as a promising method for producing large-scale graphene, the graphene layer must be transferred onto a suitable substrate for further application. In this context, thermal SiC decomposition eliminates the need for graphene transfer for synthesizing electronic devices.¹¹² Since the carbon vapor pressure is insignificant in comparison to that of silicon, when heated for a short period of time (1–20 min), the Si atoms desorb and leave behind the carbon atoms, which then rearrange to form graphitic layers.^{113,114} Emtsev et al. have demonstrated the synthesis of large-area monolayer graphene films on SiC at normal atmospheric pressure and 1650°C.¹¹⁵ The presence of argon reduces the rate of Si evaporation, resulting in a substantial enhancement in graphene surface morphology on the SiC.¹¹⁶ It is also possible to synthesize wafer-scale graphene films (mm scale) at a significantly lower temperature (1100°C) on a Ni-Cu-coated SiC substrate.¹¹⁷

Un-zipping CNTs and Other Methods

One of the most recent techniques for producing graphene involves un-zipping of carbon nanotubes (CNT) to produce graphene nanoribbons (GNRs) in a controlled way with precise dimensions. The multiwall carbon nanotubes (MWCNTs) were unzipped by various experimental methods, such as using a mixture of acids,¹¹⁸ a catalytic cutting method,¹¹⁹ electric zipping,¹²⁰ and H-based unzipping,¹²¹ etc. CNTs were utilized as the starting material for the catalytic cutting method. Carbon atoms in CNTs diffuse on the metal nanoparticles at ~ 900°C under an argon–hydrogen environment. Following that, the particles become saturated and react with H₂. The cutting can be driven in one of the two directions, depending on the particle size, resulting in the armchair or zigzag edges. Elias et al. reported using Ni or Co to longitudinally cut and open MWCNTs to create graphitic nanoribbons, typically 100–500 nm long and 15–40 nm wide.¹²²

Similarly, Wang et al. reported the top–down synthesis of GNRs using oxidative splitting with (NH₄)₂S₂O₈ in anhydrous acidic media.¹²³ This method produces GNRs with a high proportion of oxygen functionalities, which alters their

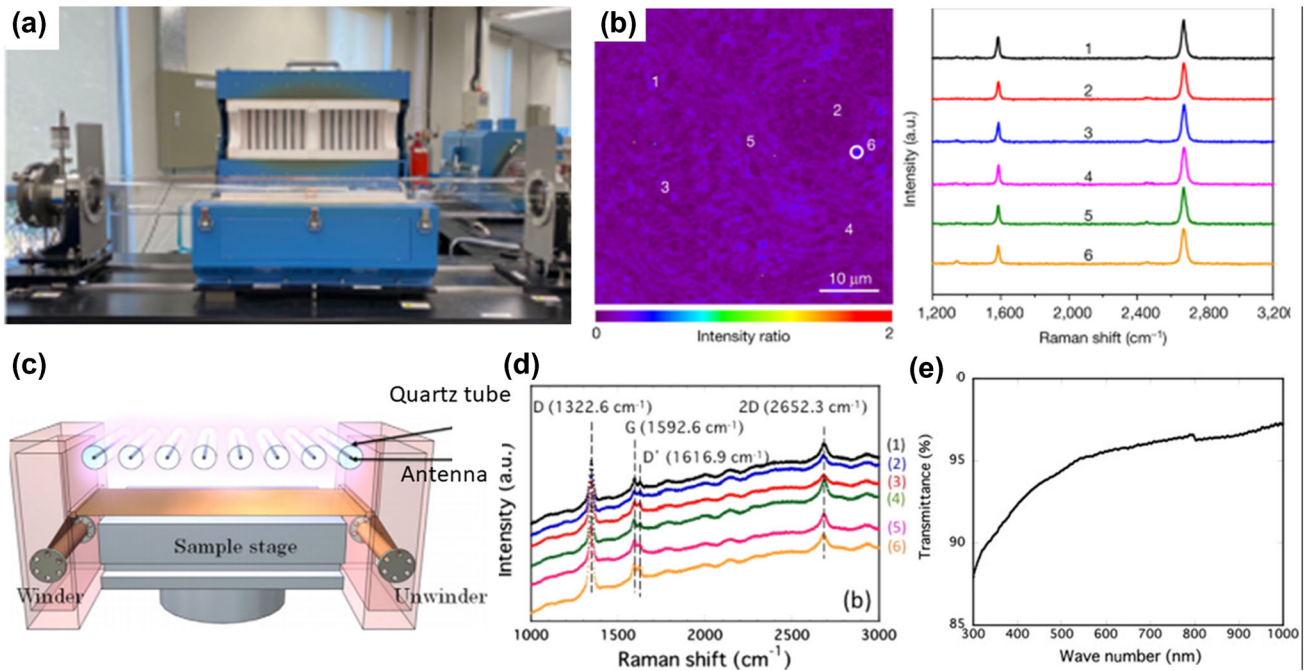


Fig. 4. (a) CVD furnace system, (b) Raman spectra and mapping of the produced graphene (reprinted with permission from Ref. 106), (c) roll-to-roll CVD apparatus, (d) Raman spectra, and (e) transmittance of the transferred graphene film (reprinted with permission from Ref. 108).

properties. Kumar et al. probably addressed this issue by irradiating MWCNTs with a laser pulse energy of 200–350 mJ. They demonstrated that their laser irradiation method is a simple way to produce GNRs with no surface contamination. Although CNT unzipping and subsequent trimming can effectively reduce the width of the GNR, the unzipping process has a low yield.¹²⁴

In another recent approach, Su et al. documented the synthesis of template-free nitrogen and sulfur co-doped 3D graphene networks (3DGNs) using the hydrothermal method.¹²⁵ Other than the hydrothermal method, the sugar-blowing method is currently the most fascinating and inexpensive technique for growing 3DGNs. Synthesis of a 3D graphene bubble network using the sugar-blowing approach following a polymeric predecessor was proposed by Wang et al.¹²⁶ Glucose is mixed with an ammonium salt and treated at 1350°C for 3 h under an Ar environment. A black foam-like, 3D self-supported graphene product was collected. Very recently, Han et al. also reported a sugar-blowing-assisted thermal reduction of GO to produce high-quality 3D porous graphene (3D-PG).¹²⁷ By adjusting the synthesis conditions, the microstructure and properties of the 3DGNs can control. For example, the pore size and porosity of 3D-PG can be tuned by changing the metal templates' pore structure in template-assisted CVD. Table II shows the comparison between the synthesis method, product, basic properties, and application of graphene.

APPLICATIONS OF GRAPHENE

Transistors and Transparent Display

The use of graphene in field-effect transistors (FET) is one of the promising applications of this material. Since graphene is a conductive material, it cannot be utilized directly in transistor applications. However, graphene in the form of nanoribbons acts as a semiconductor. This means that it can exhibit a band gap and can be turned on and off; thus, can be a crucial component of nanotransistors.¹⁴³ By patterning graphene into GNRs, the band gap can be engineered to have values up to 400 meV.¹⁴⁴ There are various methods for fabricating GNRs for FET applications, including chemical and lithographic methods. GNRs with widths ranging from 20 to 30 nm have been created using lithographic patterning. However, a recent study by Llinas et al. reported the fabrication of GNRs of only 0.95 nm in width and with a high current on/off ratio $\sim 10^5$ at RT (Fig. 5a, b).¹⁴⁵ Wu et al. reported the synthesis of a side-wall transistor with the smallest gate length of 0.34 nm and up to 1.02×10^5 on/off ratios.¹⁴⁰ The side-wall transistors were fabricated using CVD with graphene and molybdenum disulfide (MoS₂) to achieve devices below 1 nm. The mobility of graphene FET depends on the choice of substrate materials. In this context, Alam et al. created a graphene-based ferroelectric FET having a mobility $\sim 4.2 \times 10^4$ cm²/Vs, and about a 10^3 on/off ratio.¹⁴⁶

Indium tin oxide (ITO) is a transparent conducting material used in smartphones, television screens, and many touchscreen applications.

Table II. Comparison between synthesis method, product, basic properties, and application

Synthesis method	Product	Properties	Applications	Refs.
Mechanical exfoliation	Few-layer graphene (10 μm in size)	Electron mobility $\approx 10,000 \text{ cm}^2/\text{V s}$	Hall bar devices	Ref. 128
Electrochemical exfoliation	Graphene nanosheets (GNS) (500–700 nm in size)	Conductivity 13.84 S/m	GNS/polystyrene composites	Ref. 129
Metal-organic chemical vapor deposition (MOCVD)	Monolayer graphene	Optical transmittance $> 97\%$ and sheet resistance of $450 \pm 47 \Omega/\text{sq}$	Transparent conducting electrode	Ref. 130
Hummer's method	rGO (1 μm in size)	Self-healing efficiency 89% and ultra-high toughness of 141.19 MJ/m ³	PU/graphene nanocomposite for microplastic removal from water	Ref. 131
Mechanical exfoliation and Interface Functionalization	Graphene nanosheets (thickness 2.4 nm)	Elastic strain 110%	Artificial skin	Ref. 132
Wet-jet milling/liquid phase exfoliation	Single/few-layer graphene flakes	Efficiency at 12.5% and 250-W power output	Solar cell	Ref. 133
CVD	Few-layer graphene	85% optically transparent 85% and conductive Young's moduli $\approx 1100 \text{ kPa}$	Graphene tattoos	Ref. 134
Ethanol-assisted reduction treatment	rGO		Treatment of skin cancer	Ref. 135
Freeze-drying	GO aerogel foam	Conductivity $4.12 \times 10^{-4} \text{ S/cm}$	Solid state battery	Ref. 136
Gas phase synthesized graphene	Single to few-layer graphene	Water contacts $153.0^\circ \pm 3.0^\circ$	Superhydrophobic coating	Ref. 137
Electrophoretic deposition	Graphene nanosheets	Tensile strength 518 MPa, and bending strength 477 MPa	Supercapacitor	Ref. 138
Mechanical exfoliation	Graphene flakes	Mobility $130,000 \text{ cm}^2/\text{Vs}$	Spintronics	Ref. 139
CVD	Monolayer graphene (0.34 nm)	On/Off ratio 1.02×10^5	Transistor	Ref. 140
Microfluidized technique	Graphene inks	Resistance $\approx 49 \Omega/\text{cm}$	E-textile	Ref. 141
Flash Joule heating	Graphene sheets (size 13.8 nm)	34% increase in tensile strength and 25% in low-frequency noise absorption	Polyurethane foam composite	Ref. 142

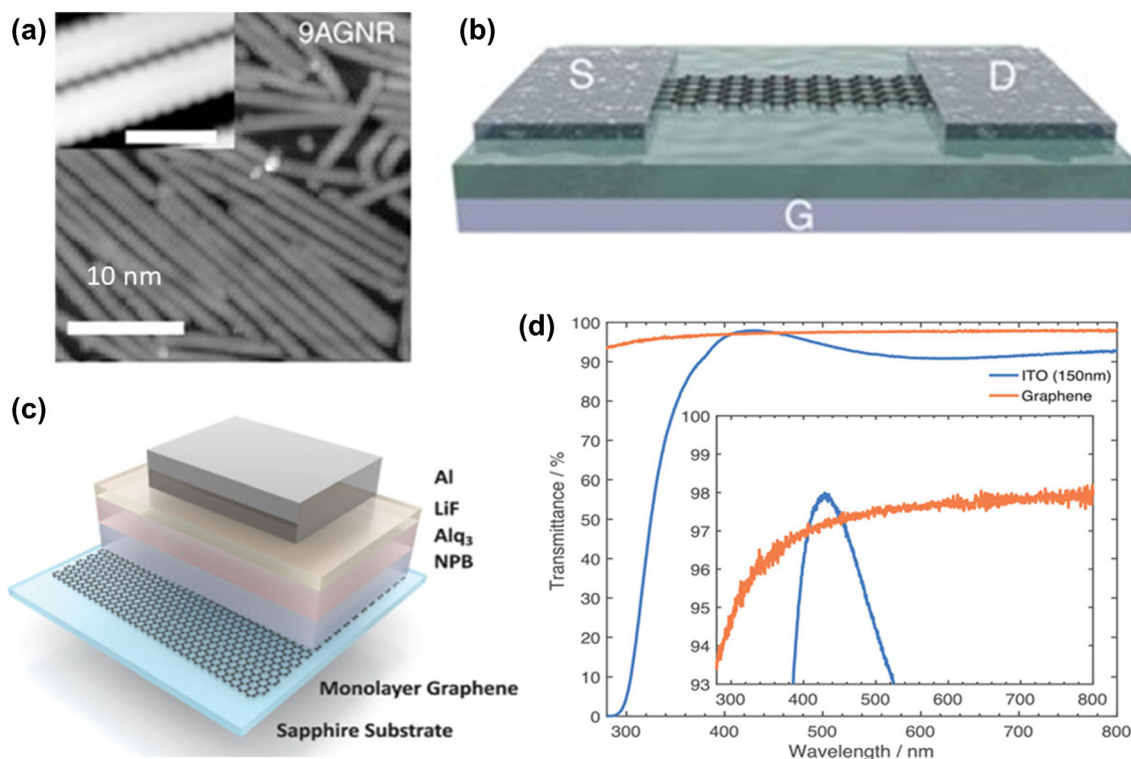


Fig. 5. (a, b) STM image of synthesized GNR on Au and a schematic of a graphene nanoribbon FET (reprinted with permission from Ref. 145), (c, d) device configuration of graphene transparent conducting electrode and optical transmittance comparison between indium tin oxide (ITO) and graphene (reprinted with permission from Ref. 130).

However, the limited availability of indium is a growing concern in the ITO market. It is anticipated that graphene will be one of the materials that will be in the highest demand for the development of future optoelectronic devices. Gautam et al. reported 85–95% transmittance with the sheet resistance in the range of 50–350 Ω/sq for monolayer graphene to F:G.¹⁴⁷ Graphene-based organic light-emitting diodes fabricated directly on a transparent sapphire substrate using metal–organic chemical vapor deposition (MOCVD) is expected to have fewer defects.¹³⁰ Figure 5b, c demonstrates the schematic and optical transmittance of > 97% from the visible to the near-infrared region identical to conventional ITO anodes.

Coatings

Silver films are extensively utilized as optical coatings; however, silver is expensive, unstable in air, and prone to oxidation, although common protective coatings have the ability to stop corrosion of silver, but change the optical properties. When compared to bare silver, the rate of corrosion of silver films covered with graphene was reduced by 66 times.¹⁴⁸ Prasai et al.¹⁴⁹ found that the graphene-covered copper exhibited a corrosion rate 7 times lower than that of bare copper in sodium sulfate solution. Similarly, in the case of Ni covered with graphene, an enhancement in the corrosion resistance by 20 times was obtained.

Graphene and its derivatives are also widely used as reinforcements in coatings to improve wear resistance.¹⁵⁰ The titanium alloy matrix has a relative wear resistance of 1 and, with an optimum graphene content of 3 g/L the resistance is increased to 12.2. Graphene-modified $\text{Al}_2\text{O}_3/\text{TiO}_2$ coatings have a 20–25% lower wear rate than non-graphene coatings.¹⁵¹ Zuo et al.¹⁵² also observed an improvement in the wear resistance of a micro-arc oxidation (MAO) coating prepared on Ti-6Al-4 V alloy with GO. They found that the MAO coating with 10 mL/L GO had comparatively superior tribocorrosion resistance, with fewer microcracks but a smoother worn surface than that of 5- and 15-mL/L GO coatings (Fig. 6a).

Graphene coatings can act as a high-energy barrier in the path of oxygen atoms.¹⁵⁵ Kang et al.¹⁵³ observed an enhancement in the oxidation resistance of Fe and Cu foils coated with rGO multilayers (Fig. 6b). Chen et al. reported similar findings, demonstrating that Cu and Si metal surfaces, when coated with graphene, are well shielded from oxidation even after being heated to 200°C for up to 4 h.¹⁵⁶

Superhydrophobic surfaces fabricated from graphene exhibit an excellent anticorrosion property.¹⁵⁴ A recent study by Miler et al. holds exciting potential for creating water-repellent coatings using gas-phase synthesized graphene, with a water contact angle of $153^\circ \pm 3^\circ$.¹³⁷ The graphene

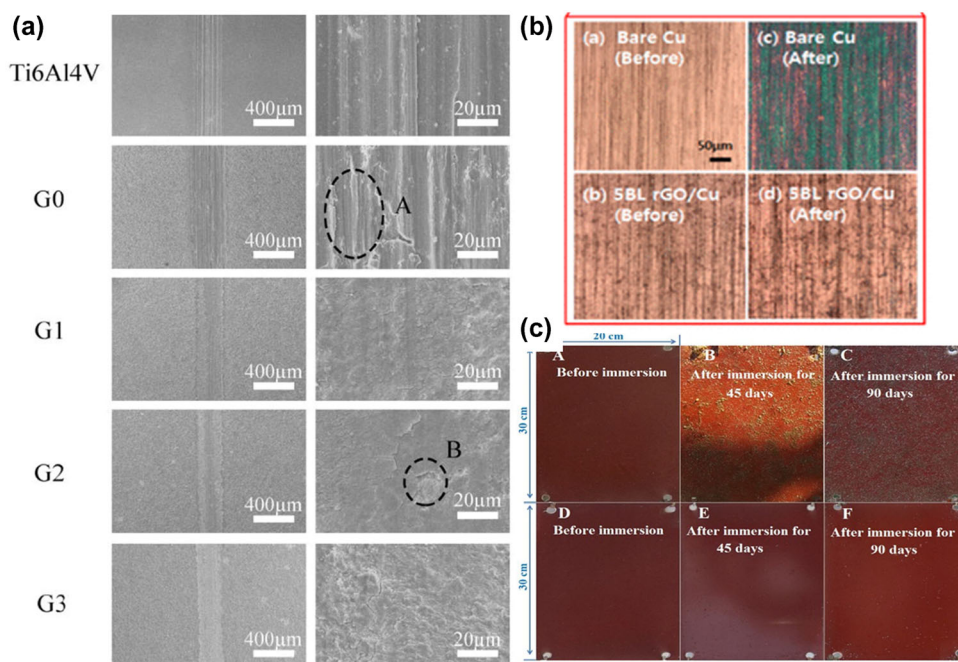


Fig. 6. (a) SEM micrographs of wear scars after tribo-corrosion experiments (G0: no GO, G1: 5 ml/l, G2: 10 ml/l, G3: 15 ml/l) (reprinted with permission from Ref. 152), (b) before and after oxidation images of bare and rGO-coated Cu foils (reprinted with permission from Ref. 153), (c) field trial images of (A–C) virgin silicone fouling release coating formulation and (D–F) PDMS/GO-Al₂O₃ coating formulation after 90 days in natural marine water (reprinted with permission from Ref. 154).

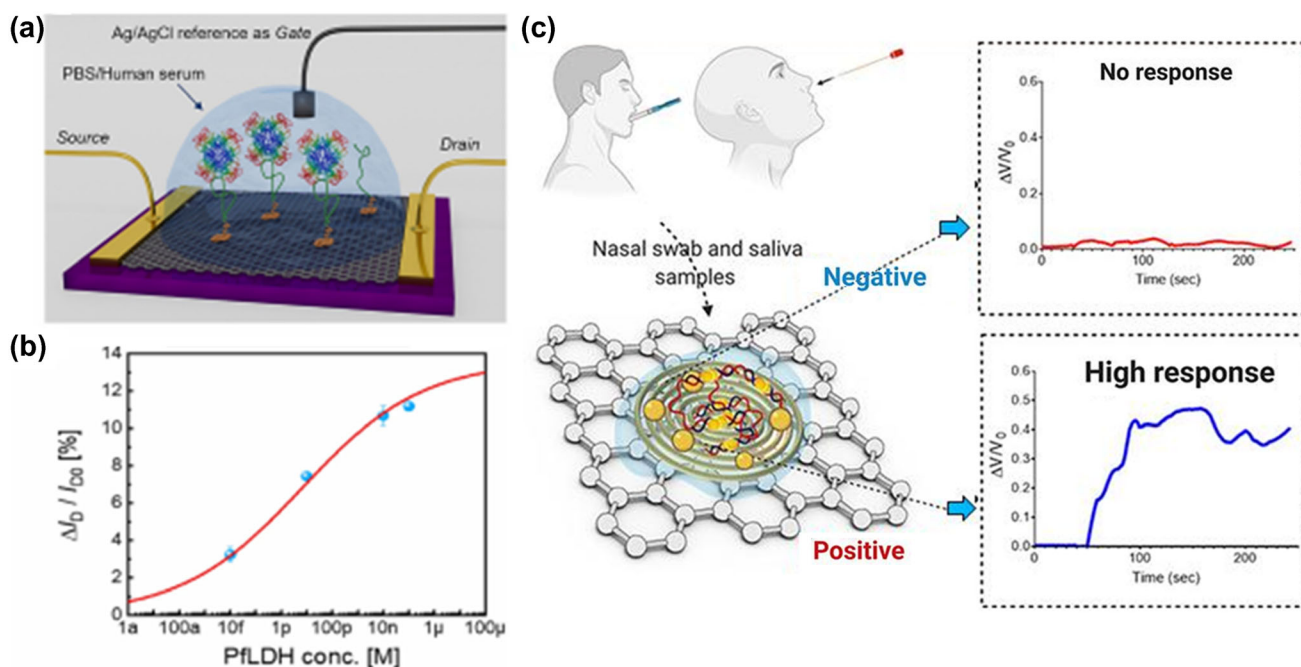


Fig. 7. (a) The 2DBioFET, (b) the results of PFLDH detection in human serum by the 2DBioFET (reprinted with permission from Ref. 157), (c) schematic of the electrochemical sensing platform for COVID-19 (reprinted with permission from Ref. 160).

grown by their reported method immediately can repel water without any chemical modifications. In another study, the use of the matrix material PDMS and rGO produced a robust superhydrophobic surface with a water contact angle of $159^\circ \pm 2^\circ$, which had self-cleaning, antifouling, and anticorrosion

properties, indicating its potential applications in the marine industry¹⁵⁴ (Fig. 6c).

Healthcare and Medicine

The biocompatibility of graphene derivatives allows their substantial use in medicine and biology.

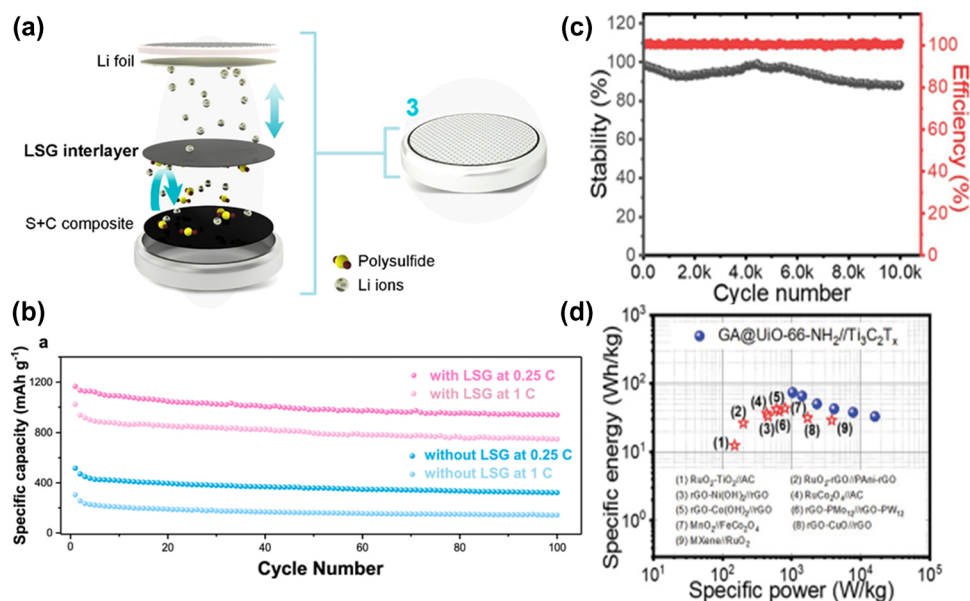


Fig. 8. (a) Schematic of a Li-S battery, (b) cycling stability of Li-S cells (reprinted with permission from Ref. 170), (c) cycling stability and coulombic efficiency measured at 5.2 A g^{-1} over 10,000 cycles, (d) Ragone plot (reprinted with permission from Ref. 171).

One of the foremost critical applications is in the early diagnosis of viruses. For example, Miranda et al. developed a graphene-based electrical biosensor for the early detection of malaria parasites (Fig. 7a, b).¹⁵⁷ In this study, an rGO-based field-effect transistor (2DBioFET) was biofunctionalized with molecules that selectively bind to a malaria biomarker, i.e., *Plasmodium falciparum* lactate dehydrogenase (PfLDH), with a detection limit down to 0.11 pg/mL . Similarly, Walters et al. developed a graphene sensor platform for rapidly diagnosing the hepatitis virus,¹⁵⁸ and reported a detection limit down to 100 pg/mL in less than 4 min, even with smaller volume samples, i.e., $5 \text{ }\mu\text{L}$. The sensor is easily adaptable to other infectious disease markers, such as hepatitis B virus, SARS-CoV-2, HIV, and many others. Roslon et al. developed a graphene drum to assess rapid antibiotic susceptibility to bacteria in drug screening.¹⁵⁹ A silicon chip containing thousands of these graphene-covered cavities was placed inside an *E. coli*-containing cuvette. The nanomotion of *E. coli* bacterium caused the suspended graphene membrane to deflect, as detected by laser interferometry, and then be converted into a soundtrack. The nanomotion of bacterium rapidly decreases in the presence of antibiotics unless the bacteria are resistant to the antibiotic.

One of the distinguishing characteristics of GO is its ability to transform stem cells into bone-generating cells known as osteoblasts. Porous 3D graphene-based scaffolds can be used for bone repair via bone tissue engineering.¹⁶¹ A porous GO scaffolding was seeded with stem cells from mouse bone marrow. After 9 days, the cell number on the 3D GO scaffolds had increased by approximately 8.5-fold,

which could be a new possible research direction to regenerate bone tissue.

Face masks have become a critical tool in the fight against the COVID-19 pandemic.^{162–165} Huang et al. discovered that, when combined with the photothermal effect of the graphene layer, the bacterial inhibition rate could be improved by up to 80% in antibacterial masks modified with laser-induced graphene, resulting in 99.998% bacterial killing efficiency within 10 min.¹⁶⁶ A sensor made of a filter paper coated with graphene could detect COVID-19 in under 5 min¹⁶⁰ (Fig. 7c). On this sensor surface, gold nanoparticles capped with ssDNA (single-stranded nucleic acids) probes specific to the SARS-CoV-2 RNA were deposited. In the presence of the SARS-CoV-2 RNA, the ssDNA hybridized with these probes. The hybridization of the viral RNA with the ssDNA sequence increases the charges at the graphene–solution interface, causing a change in the sensor’s electrical response. The sensor detected a significant increase in voltage in positive samples compared to negative samples, and confirmed the presence of virus with nearly 100% accuracy. In another study, graphene coatings have been reported as a promising contender for anti-biofilm formation to prevent infection in medical implants. When the graphene layer is loaded with usnic acid (a strong antibacterial additive), the coating provides long-term anti-biofilm protection for up to 96 h.¹⁶⁷ The coating is highly effective against *Staphylococcus aureus* and *S. epidermidis*, two common biofilm-forming bacteria on medical implants.

Table III. Market availability of graphene-based products

Company	Product	Features	Refs.
Momodesign	Helmet (FGTR Graphene 1.0)	Graphene effective thermal heat transfer	Ref. 175
Inov-8	G-series range shoes	To improve durability and strength	Ref. 178
Head	Tennis racquet (Graphene 360)	Graphene to improve flexibility and lightweight	Ref. 179
Reebok	Thermoworm + Graphene	Graphene to help consumer stay warmer in cold temperatures	Ref. 180
ZOLO	Earphone (Liberty +)	Graphene for improved sound quality	Ref. 181
Jewelpads	Jewel sanitary napkins	Graphene to help abdominal cramps, bacteria, immune system	Ref. 182
Appear Inc	Smartphone	Graphene battery-powered smartphone with innovative water-resistant technology	Ref. 183
Direct Plus	Textile collection (Graphene Plus)	Graphene for heat management and distribution	Ref. 184
Richard Mille	Watch	Lightest mechanical chronograph watch	Ref. 185
Nanometrix Materials	G1 air conditioner filters	Graphene to destroy airborne viruses and bacteria and filter certain harmful gases	Ref. 186
Dassi	Bicycle	Graphene for lightweight stiffness and heat dissipation	Ref. 187
Nanomatrix Materials	G1 Wonder face mask	COVID-19 virus filtration efficiency	Ref. 188
Graphenano	Graphenestone	This paint is a super strong and protective layer against environmental damage	Ref. 189
Biolin Scientific	Q-Sensor	Real-time surface-molecule analysis	Ref. 190
Nanomed	Biosensor (Agile)	Graphene FET as a biochemical sensor	Ref. 190
Nationwide Engineering Group, UK	Graphene concrete (Concretene)	To increase strength and reduce carbon footprint	Ref. 191
Lyten	Graphene-enhanced lithium-sulfur battery	High energy density	Ref. 192
Applied Graphene Materials	Graphene anticorrosion primer	To improve corrosion resistance	Ref. 193
Paragraf	Graphene Hall sensor	Magnetic field sensing	Ref. 194
Grapheal	Biosensor	Detection of SARS-CoV-2	Ref. 195
INBRAIN	NeuroImplants	Treat brain disorders like Parkinson's and epilepsy	Ref. 196
Neuro-electronics	Gii-Sens-3D graphene foam	Real-time health monitoring	Ref. 197
Intigrated Graphene	sensing electrode		
Versarien	Cementene	Graphene-enhanced cement	Ref. 198
National Highway UK	GiPave	Graphene enhanced asphalt	Ref. 199
SpaceBlue	Door mat and floor covering	Sustainable home furnishing	Ref. 200
AEH innovative	GelPonic	Graphene-enhanced hydrogel for vertical farming	Ref. 201
2DM	Ballistic helmet	Lightest, safest, and most efficient helmet	Ref. 202

Batteries and Supercapacitors

Lithium-based batteries are acknowledged as one of the promising substitutes for applications in energy storage systems, due to their high energy

density. One of the major reasons for the degradation in high energy density lithium-ion battery cathode materials is the formation of a dendritic structure and a solid electrolyte layer during the continuous charge–discharge cycles. Recently, Chen

et al. suppressed the formation of Li dendrites using laser induced graphene combined with a porous silicon oxide coating.¹⁶⁸ They reported an improvement in the average coulombic efficiency to 99.3% (2.0 mAh cm^{-2} at 2.0 mA cm^{-2}) compared to bare electrodes.

The lithium–sulfur (Li–S) battery is yet another promising candidate for next-generation rechargeable batteries. However, during the discharge cycle, the intermediate lithium polysulfide species dissociate in the electrolyte and diffuse between the cathode and anode, typically known as the shuttling effect, resulting in poor coulombic efficiency and rapidly reducing the capacity of the Li–S cells. The incorporation of a GO membrane to the sulfur cathode acted as an effective separator and reduced the cyclic capacity decay rate from 0.49% to 0.23%.¹⁶⁹ Laser scribed graphene, having a hierarchically 3-D porous structure, can greatly suppress polysulfide shuttling.¹⁷⁰ The resultant Li–S cell showed a high specific capacity of 1160 mAh/g with excellent cycling stability of 80.4% capacity retention after 100 cycles (Fig. 8a, b).

Graphene is frequently proposed as a substitute for activated carbon in supercapacitors due to its high relative surface area of $2,630 \text{ m}^2/\text{g}$, which is superior for storing an electrostatic charge with almost no degradation over long-term cycling. Jayaramulu et al. created a highly efficient graphene hybrid supercapacitor by combining graphene as an electrostatic electrode and a metal–organic framework as an electrochemical electrode. The device can deliver an energy density of up to 73 Wh/kg and a power density of up to 16 kW/kg , which are comparable to Pb-acid batteries and nickel metal hydride batteries. Furthermore, standard batteries (such as lithium) have a useful life of approximately 5000 cycles. However, even after 10,000 cycles, this new hybrid graphene supercapacitor retains 88% of its capacity (Fig. 8c, d).¹⁷¹

Ink-based graphene is emerging as a new technology for scalable manufacturing of printed and wearable electronics. Gaur et al. used graphene aerosol ink to print micro-supercapacitor, which showed a volumetric capacitance of 3.25 F/cm^3 at a current density of 20 mA/cm^2 with $\sim 80\%$ capacitance retention after 10,000 cycles.¹⁷² In a similar approach, Yun et al. developed graphene ink to print an extremely flexible and durable supercapacitor.¹⁷³ This micro-supercapacitor exhibited a power density of $\sim 1.13 \text{ kW/kg}$ and specific capacitance of $\sim 22 \text{ F/g}$ at a scan rate of 100 mV/s . Additionally, it is capable of being attached to power electronic devices, such as wearable skin sensors, which can be utilized for remote medical monitoring and diagnosis.

GRAPHENE COMMERCIALIZATION FROM LABORATORY TO MARKET

The commercialization of graphene is moving quite rapidly, with several real-world products on the horizon, and this trend is expected to accelerate in the coming years. For instance, in the sports industry, graphene is used to produce helmets, clothing, and tennis racquets.¹⁷⁴ Combining the mechanical and thermal benefits of graphene, an Italian-made graphene-enhanced motorcycle helmet was released in October 2016 in collaboration with the Italian Institute of Technology and the luxury design firm, Momodesign.¹⁷⁵ Graphene is applied as a coating to the exterior of the helmet, resulting in enhanced heat dissipation and increased user comfort. Graphene can improve the energy distribution and weight of a tennis racquet, as well as the speed and stability of the serve.¹⁷⁶ The tennis equipment manufacturer, Head, has already developed Graphene 360, a series of graphene-enhanced commercially available racquets. The British sportswear manufacturer, Inov-8, has produced the G-Series range of graphene-enhanced shoes as well as a pair of graphene-infused hiking boots. Utilizing graphene fibers in textiles produces antibacterial, antistatic clothing that can retain heat and block UV rays.¹⁷⁷ Companies such as Reebok, Direct Plus, and Versarien are already working on launching a new apparel collection that uses graphene in fabrics to help retain heat. Table III shows graphene-based products available in the market.

SUMMARY

A number of advantages of graphene, including its high surface area, chemical stability, thermal and electrical conductivities, super-hydrophobicity, flexibility, and so on have been discussed to illustrate the viability of bridging the nano-scale features of graphene to practical human-scale applications. To aid in the ongoing advancement of graphene-based materials and devices, this paper reviews the recent advances in their synthesis and applications. In terms of synthesis, various approaches have been successfully developed, indicating the feasibility of producing high-performance, high-quality, and large-area graphene. Exfoliation, chemical reduction of GO, CVD and thermal degradation of SiC, unzipping of CNTs, and other processes are among them. The CVD growth technique, among these, can generate large sheets of graphene with few or no defects and good conductivity; however, it must be taken into consideration that the quality of the material can be highly influenced by the process parameters used during the CVD growth. The exfoliation approach is compatible with industry-scale manufacturing of

graphene powder, with certain methods yielding more than 50%. The qualities and performance of synthesized graphene have been demonstrated to be substantially reliant on the type of reducing agents and the synthetic process used. In terms of its practical uses, the properties of graphene have garnered much interest in a wide variety of different application domains. Graphene is commonly employed in transparent displays due to its excellent conductivity and flexibility. Because of its high sensitivity, graphene is utilized as a sensor in medical devices, particularly to detect certain viruses such as COVID-19 and malaria. Graphene is used in protective coatings for metals due to its corrosion and oxidation resistance, and, due to its high surface area and nonflammable nature, it is used as an electrode material for electrochemical energy storage devices, such as lithium batteries and supercapacitors to improve device performance when compared to those that use traditional carbon as electrode materials.

ACKNOWLEDGEMENTS

The authors acknowledge the financial support of the Science and Engineering Research Board (SERB), India (Grant No. EMR/2016/001282).

CONFLICT OF INTEREST

The authors declare that they have no known competing financial interests or personal relationships that could have appeared to influence the work reported in this paper.

REFERENCES

1. A. Geim, and K. Novoselov, *Nat. Mater.* 6, 183. (2007).
2. Y. Zhang, T. Tang, C. Girit, Z. Hao, C. Martin, A. Zettl, F. Crommie, R. Shen, and F. Wang, *Nature* 459, 820. (2009).
3. A. Balandin, S. Ghosh, W. Bao, I. Calizo, D. Teweldebrhan, F. Miao, and N. Lau, *Nano Lett.* 8, 902. (2008).
4. P. Blake, P. Brimicombe, R. Nair, T. Booth, D. Jiang, F. Schedin, L. Ponomarenko, S. Morozov, H. Gleeson, E. Hill, and A. Geim, *Nano Lett.* 8, 1704. (2008).
5. T.J. Booth, P. Blake, R.R. Nair, D. Jiang, E.W. Hill, U. Bangert, A. Bleloch, M. Gass, K.S. Novoselov, M.I. Katsnelson, and A.K. Geim, *Nano Lett.* 8, 2442. (2008).
6. P. Somani, P. Savita, and U. Masayoshi, *Chem. Phys. Lett.* 430, 56. (2006).
7. A.N. Obratsov, E.A. Obratsova, A.V. Tyurnina, and A.A. Zolotukhin, *Carbon* 45, 2017. (2007).
8. G. Eda, G. Fanchini, and M. Chhowalla, *Nat. Nanotechnol.* 3, 270. (2008).
9. X. Li, W. Cai, J. An, S. Kim, J. Nah, D. Yang, R. Piner, and R. Ruoff, *Science* 324, 1312. (2009).
10. S. Bae, H. Kim, Y. Lee, X. Xu, J. Park, Y. Zheng, J. Balakrishnan, T. Lei, H.R. Kim, Y. Song, Y. Kim, K. Kim, B. Ozyilmaz, J. Ahn, B. Hong, and S. Iijima, *Nat. Nanotechnol.* 5, 574. (2010).
11. K. Paton, E. Varrla, C. Backes, and J. Coleman, *Nat. Mater.* 13, 624. (2014).
12. D.X. Luong, K.V. Bets, W.A. Algozeeb, M.G. Stanford, C. Kittrell, W. Chen, R.V. Salvatierra, M. Ren, E.A. McHugh, P.A. Advincula, Z. Wang, M. Bhatt, H. Guo, V. Mancevski, R. Shahsavari, B.I. Yakobson, and J.M. Tour, *Nature* 577, 647. (2020).
13. F. Giannazzo, R. Dagher, E. Schilirò, S.E. Panasci, G. Greco, G. Nicotra, F. Roccaforte, S. Agnello, J. Brault, Y. Cordier, and A. Michon, *Nanotechnology* 32, 015705. (2020).
14. A. K. Sood, I. Lund, Y.R. Puri, H. Efstathiadis, P. Haldar, N.K. Dhar, J. Lewis, M. Dubey, E. Zakar, P. Wijewarnasuriya, and D.L. Polla and M. Fritze, London, UK: InTech, 38 (2015).
15. Y. Li, K. Tantiwanichapan, A.K. Swan, and R. Paiella, *Nanophotonics* 9, 1901. (2020).
16. M.P. Kumar, P.M. Laxmeesha, S. Ray, and C. Srivastava, *Appl. Surf. Sci.* 533, 147512. (2020).
17. P. Fu, G.L. Teri, X.L. Chao, J. Li, Y.H. Li, and H. Yang, *Coatings* 10, 1. (2020).
18. C.V.M. Gopi, R. Vinodh, S. Sambasivam, I.M. Obaidat, and H.J. Kim, *J. Energy Storage* 27, 101035. (2020).
19. B. Taheri, N.Y. Nia, A. Agresti, S. Pescetelli, C. Ciceroni, R. Castillo, L. Cinà, S. Bellani, F. Bonaccorso, and A. Di Carlo, *2D Mater.* 5, 045034. (2018).
20. S. Rani, and S.J. Ray, *Carbon* 173, 493. (2021).
21. A. Ghamkhari, S. Abbaspour-Ravasjani, M. Talebi, H. Hamishehkar, and M.R. Hamblin, *Int. J. Biol. Macromol.* 169, 521. (2021).
22. L.M. Viculis, J.J. Mack, and R.B. Kaner, *Science* 299, 1361. (2003).
23. M. Yi, and Z. Shen, *J. Mater. Chem. A* 3, 11700. (2015).
24. B. Hu, H. Ago, Y. Ito, K. Kawahara, M. Tsuji, E. Magome, K. Sumitani, N. Mizuta, K.I. Ikeda, and S. Mizuno, *Carbon* 50, 57. (2012).
25. J.D. Wood, S.W. Schmucker, A.S. Lyons, E. Pop, and J.W. Lyding, *Nano Lett.* 11, 4547. (2011).
26. X. Xu, C. Liu, Z. Sun, T. Cao, Z. Zhang, E. Wang, Z. Liu, and K. Liu, *Chem. Soc. Rev.* 47, 3059. (2018).
27. J.B. Oostinga, H.B. Heersche, X. Liu, A.F. Morpurgo, and L.M. Vandersypen, *Nat. Mater.* 7, 151. (2008).
28. S.V. Morozov, K.S. Novoselov, F. Schedin, D. Jiang, A.A. Firsov, and A.K. Geim, *Phys. Rev. B* 72, 201401. (2005).
29. J. Hass, W.A. De Heer, and E.H. Conrad, *J. Phys. Condens. Matter* 20, 323202. (2008).
30. Y. Huang, X. Li, H. Cui, and Z. Zhou, *Curr. Graphene Sci.* 2, 97. (2018).
31. Y. Shan, Y. Li, D. Huang, Q. Tong, W. Yao, W.T. Liu, and S. Wu, *Sci. Adv.* 4, 1. (2018).
32. B.R. Wu, *Appl. Phys. Lett.* 98, 263107. (2011).
33. K. Tang, R. Qin, J. Zhou, H. Qu, J. Zheng, R. Fei, H. Li, Q. Zheng, Z. Gao, and J. Lu, *J. Phys. Chem. C* 115, 9458. (2011).
34. S. Ghosh, W. Bao, D.L. Nika, S. Subrina, E.P. Pokatilov, C.N. Lau, and A.A. Balandin, *Nat. Mater.* 9, 555. (2010).
35. C. Bouhafs, V. Darakchieva, I.L. Persson, A. Tiberj, P.O.Å. Persson, M. Paillet, A.A. Zahab, and R. Yakimova, *J. Appl. Phys.* 117, 085701. (2015).
36. C. Weiwei, A.L. Moore, Y. Zhu, X. Li, S. Chen, L. Shi, and R.S. Ruoff, *Nano Lett* 10, 1654. (2010).
37. M. Hoda, and A.A. Balandin, *J. Raman Spectrosc.* 49, 106. (2018).
38. P. Manuel, M.C. Rosamond, P. Tovee, M.C. Petty, D.A. Zeze, V. Falko, and O.V. Kolosov, *Nano Lett.* 12, 2906. (2012).
39. L. Jae-Ung, D. Yoon, H. Kim, S.W. Lee, and H. Cheong, *Phys. Rev. B* 83, 08419. (2011).
40. D.S. Ghosh, I. Calizo, D. Teweldebrhan, E.P. Pokatilov, D.L. Nika, A.A. Balandin, W. Bao, F. Miao, and C.N. Lau, *Appl. Phys. Lett.* 92, 151911. (2008).
41. J.H. Seol, I. Jo, A.L. Moore, L. Lindsay, Z.H. Aitken, M.T. Pettes, X. Li, Z. Yao, R. Huang, D. Broido, N. Mingo, R.S. Ruoff, and L. Shi, *Science* 328, 213. (2010).
42. A.L. Falkovsky, and A. Leonid, *J. Phys. Conf. Series* 129, 012004. (2008).
43. R.R. Nair, P. Blake, A.N. Grigorenko, K.S. Novoselov, T.J. Booth, T. Stauber, N.M.R. Peres, and A.K. Geim, *Science* 320, 1308. (2008).
44. Y. Zhu, S. Murali, W. Cai, X. Li, J.W. Suk, J.R. Potts, and R.S. Ruoff, *Adv. Mater.* 22, 3906. (2010).

45. L. ZhiBo, Z. XiaoLiang, Y. XiaoQing, C. YongSheng, and T. JianGuo, *Chin Sci Bull* 57, 2971. (2012).
46. M.K. Kavitha, and M. Jaiswal, *Asian J Phys.* 25, 809. (2016).
47. Z.H. Ni, H.M. Wang, J. Kasim, H.M. Fan, T. Yu, Y.H. Wu, Y.P. Feng, and Z.X. Shen, *Nano Lett.* 7, 2758. (2007).
48. M. Bruna, and S. Borini, *Appl. Phys. Lett.* 94, 1. (2009).
49. E.O. Martínez, M. Gabás, L. Barrutia, A. Pesquera, A. Centeno, S. Palanco, A. Zurutuza, and C. Algora, *Nanoscale* 7, 1491. (2015).
50. A. Hill, S.A. Mikhailov, and K. Ziegler, *Europhys. Lett.* 87, 27005. (2009).
51. A. Zandiatashbar, G.H. Lee, S.J. An, S. Lee, N. Mathew, M. Terrones, T. Hayashi, C.R. Picu, J. Hone, and N. Koratkar, *Nat. Commun.* 5, 1. (2014).
52. C. Lee, X. Wei, J.W. Kysar, and J. Hone, *Science* 321, 385. (2008).
53. H. Nishihara, T. Simura, S. Kobayashi, K. Nomura, R. Berenguer, M. Ito, M. Uchimura, H. Iden, K. Arihara, A. Ohma, and Y. Hayasaka, *Adv. Func. Mater.* 26, 6418. (2016).
54. C.N.R. Rao, A.K. Sood, R. Voggu, and K.S. Subrahmanyam, *J. Phys. Chem. Lett.* 1, 572. (2010).
55. P. Navajas, N.G. Asenjo, R. Santamaría, R. Menendez, A. Corma, and H. García, *Langmuir* 29, 13443. (2013).
56. S. Zhang, H. Wang, J. Liu, and C. Bao, *Mater. Lett.* 261, 127098. (2020).
57. M.D. Stoller, S. Park, Y. Zhu, J. An, and R.S. Ruoff, *Nano Lett.* 8, 3498. (2008).
58. D.L. Rosa, J. Sun, N. Lindvall, M. Cole, Y. Nam, M. Löffler, E. Olsson, K. Teo, and A. Yurgens, *Appl. Phys. Lett.* 102, 022101. (2013).
59. H.J. Park, J. Meyer, S. Roth, and V. Skákalová, *Carbon* 48, 1088. (2010).
60. Q.B. Zheng, M.M. Gudarzi, S.J. Wang, Y. Geng, Z. Li, and J.K. Kim, *Carbon* 49, 2916. (2011).
61. K.I. Bolotin, K.J. Sikes, Z. Jiang, M. Klima, G. Fudenberg, J. Hone, P. Kim, and H.L. Stormer, *Solid State Commun.* 146, 351. (2008).
62. X. Li, K.M. Borysenko, M.B. Nardelli, and K.W. Kim, *Phys. Rev. B* 84, 195453. (2011).
63. Y. Xue, B. Wu, Y. Guo, L. Huang, L. Jiang, J. Chen, D. Geng, Y. Liu, W. Hu, and G. Yu, *Nano Res.* 4, 1208. (2011).
64. S. Gupta, P. Joshi, and J. Narayan, *Carbon* 170, 327. (2020).
65. H. Li, H. Ying, X. Chen, D.L. Nika, A.I. Cocemasov, W. Cai, A.A. Balandin, and S. Chen, *Nanoscale* 6, 13402. (2014).
66. V. Talesara, P.D. Garman, J.L. Lee, and W. Lu, *IEEE Trans. Power Electron.* 35, 578. (2019).
67. J. Chen, and L. Li, *J. Market. Res.* 9, 13740. (2020).
68. N.K. Mahanta, A.R. Abramson, *13th intersociety conference on thermal and thermomechanical phenomena in electronic systems*, IEEE, 1 (2012).
69. J.U. Lee, D. Yoon, and H. Cheong, *Nano Lett.* 12, 4444. (2012).
70. D.A. Dikin, S. Stankovich, E.J. Zimney, R.D. Piner, G. Dommett, G. Evmenenko, S. Nguyen, and R.S. Ruoff, *Nature* 448, 457. (2007).
71. C. Gómez-Navarro, M. Burghard, and K. Kern, *Nano Lett.* 8, 2045. (2008).
72. A. Liu, and Q. Peng, *Micromachines* 9, 440. (2018).
73. B. Mortazavi, Y. Rémond, S. Ahzi, and V. Toniazzo, *Comput. Mater. Sci.* 53, 298. (2012).
74. S. Wan, Y. Chen, Y. Wang, G. Li, G. Wang, L. Liu, J. Zhang, Y. Liu, Z. Xu, A. Tomsia, L. Jiang, and Q. Cheng, *Matter* 1, 389. (2019).
75. X. Lu, M. Yu, H. Huang, and R.S. Ruoff, *Nanotechnology* 10, 269. (1999).
76. K.S. Novoselov, D. Jiang, F. Schedin, T.J. Booth, V.V. Khotkevich, S.V. Morozov, and A.K. Geim, *Proc. Natl. Acad. Sci.* 102, 10451. (2005).
77. Y. Huang, Y. Pan, R. Yang, L. Bao, L. Meng, H. Luo, and Y. Cai, *Nat. Commun.* 11, 1. (2020).
78. M.S. Dresselhaus, and P.T. Araujo, *ACS Nano* 4, 6297. (2010).
79. B. Jayasena, and S. Subbiah, *Nanoscale Res. Lett.* 6, 1. (2011).
80. R. Narayan, J. Lim, T. Jeon, D.J. Li, and S.O. Kim, *Carbon* 119, 555. (2017).
81. X. Zhang, L. Wang, Q. Lu, and D.L. Kaplan, *ACS Appl. Mater. Interfaces.* 10, 22924. (2018).
82. Y. Zhang, and Y. Xu, *Adv. Func. Mater.* 29, 1902171. (2019).
83. A. Islam, B. Mukherjee, K.K. Pandey, and A.K. Keshri, *ACS Nano* 15, 1775. (2021).
84. D.C. Marcano, D.V. Kosynkin, J.M. Berlin, A. Sinitskii, Z. Sun, A. Slesarev, L.B. Alemany, W. Lu, and J.M. Tour, *ACS Nano* 4, 4806. (2010).
85. V.C. Tung, M.J. Allen, Y. Yang, and R.B. Kaner, *Nat. Nanotechnol.* 4, 25. (2009).
86. R. Ramachandran, S. Felix, G.M. Joshi, B.P. Raghupathy, S.K. Jeong, and A.N. Grace, *Mater. Res. Bull.* 48, 3834. (2013).
87. S. Park, Y. Hu, J.O. Hwang, E.S. Lee, L.B. Casabianca, W. Cai, J.R. Potts, H.W. Ha, S. Chen, J. Oh, S.O. Kim, Y.H. Kim, Y. Ishii, and R.S. Ruoff, *Nat. Commun.* 3, 1. (2012).
88. M.J. Fernández-Merino, L. Guardia, J.I. Paredes, S. Villar-Rodil, P. Solís-Fernández, A. Martínez-Alonso, and J.M.D. Tascón, *J. Phys. Chem. C* 114, 6426. (2010).
89. S. Abdolhosseinzadeh, H. Asgharzadeh, and H.S. Kim, *Sci. Rep.* 5, 1. (2015).
90. R.K. Upadhyay, N. Sooin, G. Bhattacharya, S. Saha, A. Barman, and S.S. Roy, *Mater. Lett.* 160, 355. (2015).
91. S. Mahata, A. Sahu, P. Shukla, A. Rai, M. Singh, and V.K. Rai, *New J. Chem.* 42, 19945. (2018).
92. S. Park, and R.S. Ruoff, *Nat. Nanotechnol.* 4, 217. (2009).
93. P.W. Sutter, J.I. Flege, and E.A. Sutter, *Nat. Mater.* 7, 406. (2008).
94. J. Coraux, M. Engler, C. Busse, D. Wall, N. Buckanie, R. Van Gastel, B. Poelsema, and T. Michely, *New J. Phys.* 11, 023006. (2009).
95. M. Gao, Y. Pan, L. Huang, H. Hu, L.Z. Zhang, H.M. Guo, S.X. Du, and H.J. Gao, *Appl. Phys. Lett.* 98, 033101. (2011).
96. P. Sutter, J.T. Sadowski, and E. Sutter, *Phys. Rev. B* 80, 245411. (2009).
97. A. Varykhalov, and O. Rader, *Phys. Rev. B* 80, 035437. (2009).
98. S.Y. Kwon, C.V. Ciobanu, V. Petrova, V.B. Shenoy, J. Bareno, V. Gambin, I. Petrov, and S. Kodambaka, *Nano Lett.* 9, 3985. (2009).
99. R. Addou, A. Dahal, P. Sutter, and M. Batzill, *Appl. Phys. Lett.* 100, 021601. (2012).
100. K.A. Simonov, N.A. Vinogradov, A.S. Vinogradov, A.V. Generalov, E.M. Zagrebina, G.I. Svirskiy, A.A. Cafolla, T. Carpy, J.P. Cunniffe, T. Taketsugu, and A. Lyalin, *ACS Nano* 9, 8997. (2015).
101. M. Ishihara, Y. Koga, J. Kim, K. Tsugawa, and M. Hasegawa, *Mater. Lett.* 65, 2864. (2011).
102. K.M. Reddy, A.D. Gledhill, C.H. Chen, J.M. Drexler, and N.P. Padture, *Appl. Phys. Lett.* 98, 113117. (2011).
103. A. Dahal, and M. Batzill, *Nanoscale* 6, 2548. (2014).
104. Q. Yu, J. Lian, S. Siriponglert, H. Li, Y.P. Chen, and S.S. Pei, *Appl. Phys. Lett.* 93, 113103. (2008).
105. Y. Zhang, L. Gomez, F.N. Ishikawa, A. Madaria, K. Ryu, C. Wang, A. Badmaev, and C. Zhou, *J. Phys. Chem. Lett.* 1, 3101. (2010).
106. M. Wang, M. Huang, D. Luo, Y. Li, M. Choe, W.K. Seong, M. Kim, S. Jin, M. Wang, S. Chatterjee, and Y. Kwon, *Nature* 596, 519. (2021).
107. S. Bae, H. Kim, Y. Lee, X. Xu, J.S. Park, Y. Zheng, J. Balakrishnan, T. Lei, H.R. Kim, Y.I. Song, and Y.J. Kim, *Nat. Nanotechnol.* 5, 574. (2010).
108. T. Yamada, M. Ishihara, J. Kim, M. Hasegawa, and S. Iijima, *Carbon* 50, 2615. (2012).
109. H. Uchida, H.R. Aryal, S. Adhikari, and M. Umeno, *J. Phys. Sci. Appl.* 6, 34. (2016).

110. Y. Kim, W. Song, S.Y. Lee, C. Jeon, W. Jung, M. Kim, and C.Y. Park, *Appl. Phys. Lett.* 98, 263106. (2011).
111. J. Kim, M. Ishihara, Y. Koga, K. Tsugawa, M. Hasegawa, and S. Iijima, *Appl. Phys. Lett.* 98, 091502. (2011).
112. J. Choi, H. Lee, and S. Kim, *J. Phys. Chem. C* 114, 13344. (2010).
113. D.V. Badami, *Carbon* 3, 53. (1965).
114. A.J. Van Bommel, J.E. Crombeen, and A. Van Tooren, *Surf. Sci.* 48, 463. (1975).
115. K.V. Emtsev, A. Bostwick, K. Horn, J. Jobst, G.L. Kellogg, L. Ley, J.L. McChesney, T. Ohta, S.A. Reshanov, J. Röhrl, and E. Rotenberg, *Nat. Mater.* 8, 203. (2009).
116. J. Jobst, D. Waldmann, F. Speck, R. Hirner, D.K. Maude, T. Seyller, and H.B. Weber, *Solid State Commun.* 151, 1061. (2011).
117. A. Pradeepkumar, M. Amjadipour, N. Mishra, C. Liu, M.S. Fuhrer, A. Bendavid, F. Isa, M. Zielinski, H.I. Sirikumara, T. Jayasekara, and D.K. Gaskill, *ACS Appl. Nano Mater.* 3, 830. (2019).
118. Y.S. Li, J.L. Liao, S.Y. Wang, and W.H. Chiang, *Sci. Rep.* 6, 1. (2016).
119. J. Wang, L. Ma, Q. Yuan, L. Zhu, and F. Ding, *Angew. Chem.* 123, 8191. (2011).
120. Q.F. Zheng, Y. Guo, Y. Liang, and Q. Shen, *ACS Appl. Nano Mater.* 3, 4708. (2020).
121. L. Tsetseris, and S.T. Pantelides, *Appl. Phys. Lett.* 99, 143119. (2011).
122. A.L. Elías, A.R. Botello-Méndez, D. Meneses-Rodríguez, V. Jehová González, D. Ramirez-Gonzalez, E. Munoz-Sandoval, P.M. Ajayan, H. Terrones, and M. Terrones, *Nano Lett.* 10, 366–458. (2010).
123. T. Wang, Z. Wang, R.V. Salvatierra, E. McHugh, and T.M. Tour, *Carbon* 158, 615. (2020).
124. P. Kumar, L.S. Panchakarla, and C.N.R. Rao, *Nanoscale* 3, 2127. (2011).
125. Y. Su, Y. Zhang, X. Zhuang, S. Li, D. Wu, F. Zhang, and X. Feng, *Carbon* 62, 296. (2013).
126. X. Wang, Y. Zhang, C. Zhi, X. Wang, D. Tang, Y. Xu, Q. Weng, X. Jiang, M. Mitome, D. Golberg, and Y. Bando, *Nat. Commun.* 4, 1. (2013).
127. F. Han, O. Qian, B. Chen, H. Tang, and M. Wang, *J. Alloy. Compd.* 730, 386. (2018).
128. K.S. Novoselov, A.K. Geim, S.V. Morozov, D. Jiang, Y. Zhang, S.V. Dubonos, I.V. Grigorieva, and A.A. Firsov, *Science* 666, 5696. (2004).
129. N. Liu, L. Fang, H. Wu, Y. Liu, C. Zhang, and J. Chen, *Adv. Func. Mater.* 18, 1518. (2008).
130. Z. Weng, S.C. Dixon, L. Lee, C.J. Humphreys, I. Guiney, O. Fenwick, and W.P. Gillin, *Adv. Mater.* 10, 2101675. (2022).
131. Y. Wang, G. Su, J. Li, Q. Guo, Y. Miao, and X. Zhang, *Nano Lett.* 22, 5409. (2022).
132. P. Xiao, W. Zhou, Y. Liang, S. Kuo, Q. Yang, and T. Chen, *Adv. Func. Mater.* 32, 1. (2022).
133. S. Pescetelli, A. Agresti, G. Viskadourous, S. Razza, K. Rogdakis, I. Kalogerakis, E. Spiliarotis, et al., *Nat. Energy* 7, 597. (2022).
134. D. Kireev, K. Sel, B. Ibrahim, N. Kumar, A. Akbari, R. Jafari, and D. Akinwande, *Nat. Nanotechnol.* 17(8), 864. (2022).
135. Y. Wu, J. Yang, A.V. Teijlingen, A. Berardo, I. Corridori, J. Feng, J. Xu, and A. Mata, *Adv. Func. Mater.* 2205802, 1. (2022).
136. X. Zhou, P. Lv, M. Li, J. Xu, G. Cheng, N. Yuan, and J. Ding, *Langmuir* 38, 3257. (2022).
137. M. Miller, M. Parkinson, and A. Dato, *ACS Mater. Lett.* 4, 995. (2022).
138. D. Pandey, K.S. Kumar, L.N. Henderson, G. Suarez, P. Vega, H.R. Salvador, L. Roberson, and J. Thomas, *Small* 18, 2107053. (2022).
139. V. Guarochico-Moreira, J.L. Sambricio, K. Omari, C.R. Anderson, D.A. Bandurín, J.C. Toscano-Figueroa, N. Natera-Cordero, and I. Vera-Marun, *Nano Lett.* 22, 935. (2022).
140. F. Wu, H. Tian, Y. Shen, Z. Hou, J. Ren, G. Gou, Y. Sun, Y. Yang, and T. Ren, *Nature* 603, 259. (2022).
141. M.R. Islam, S. Afroj, C. Beach, M.H. Islam, C. Parraman, A. Abdelkader, A.J. Casson, K.S. Novoselov, and N. Karim, *Isience* 25, 1. (2022).
142. K.W. Wyss, R. De Kleine, R.L. Couvreur, A. Kiziltas, D.F. Mielewski, and J.M. Tour, *Commun. Eng.* 1, 1. (2022).
143. S. Lone, A. Bhardwaj, A.K. Pandit, S. Gupta, and S. Mahajan, *J. Electron. Mater.* 50, 3169. (2021).
144. M.Y. Han, B. Özyilmaz, Y. Zhang, and P. Kim, *Phys. Rev. Lett.* 98, 206805. (2007).
145. J.P. Llinas, A. Fairbrother, G. Borin Barin, W. Shi, K. Lee, S. Wu, B. Yong Choi, R. Braganza, J. Lear, N. Kau, and W. Choi, *Nature Commun.* 8, 1. (2017).
146. I. Alam, K. Sa, S. Das, B.V.R.S. Subramanyam, S. Subudhi, M. Mandal, S. Patra, B. Samanta, R.R. Sahu, S. Swain, and A. Mahapatra, *Solid State Commun.* 340, 114533. (2021).
147. M. Gautam, Z. Shi, and A.H. Jayatissa, *Sol. Energy Mater. Sol. Cells* 163, 1. (2017).
148. Y. Zhao, Y. Xie, Y. Hui, L. Tang, W. Jie, Y. Jiang, L. Xu, S.P. Lau, and Y. Chai, *J. Mater. Chem. C* 1, 4956. (2013).
149. D. Prasai, J.C. Tuberquia, R.R. Harl, G.K. Jennings, and K.I. Bolotin, *ACS Nano* 6, 1102. (2012).
150. W. Liu, C. Blawert, M.L. Zheludkevich, Y. Lin, M. Talha, Y. Shi, and L. Chen, *J. Alloys Compd.* 789, 1007. (2019).
151. L. Wang, S. Liu, J. Gou, Q. Zhang, F. Zhou, Y. Wang, and R. Chu, *Appl. Surf. Sci.* 492, 272. (2019).
152. Y. Zuo, T. Li, P. Yu, Z. Zhao, X. Chen, Y. Zhang, and F. Chen, *Appl. Surf. Sci.* 480, 26. (2019).
153. D. Kang, J.Y. Kwon, H. Cho, J.H. Sim, H.S. Hwang, C.S. Kim, Y.J. Kim, R.S. Ruoff, and H.S. Shin, *ACS Nano* 6, 7763. (2012).
154. M.S. Selim, S.A. El-Safty, N.A. Fatthallah, and M.A. Shenashen, *Progr. Organ. Coat.* 121, 160. (2018).
155. M. Schriver, W. Regan, W.J. Gannett, A.M. Zaniewski, M.F. Crommie, and A. Zettl, *ACS Nano* 7, 5763. (2013).
156. S. Chen, L. Brown, M. Levendorf, W. Cai, S.Y. Ju, J. Edgeworth, X. Li, C.W. Magnuson, A. Velamakanni, R.D. Piner, and J. Kang, *ACS Nano* 5, 1321. (2011).
157. G. Figueroa-Miranda, Y. Liang, M. Suranglikar, M. Stadler, N. Samane, M. Tintelott, Y. Lo, J.A. Tanner, X.T. Vu, J. Knoch, and S. Ingebrandt, *Biosens. Bioelectron.* 208, 114219. (2022).
158. F. Walters, G. Burwell, J.J. Mitchell, M.M. Ali, E. Daghigh Ahmadi, A.B. Mostert, C.A. Jenkins, S. Rozhko, O. Kazakova, and O.J. Guy, *Adv. NanoBiomed. Res.* 2, 2100140. (2022).
159. I.E. Rosłoń, A. Japaridze, P.G. Steeneken, C. Dekker, and F. Alijani, *Nat. Nanotechnol.* 17, 1. (2022).
160. M. Alafeef, K. Dighe, P. Moitra, and D. Pan, *ACS Nano* 14, 17028. (2020).
161. Y. Chen, X. Su, D. Esmail, E. Buck, S.D. Tran, T. Szkopek, and M. Cerruti, *Carbon* 189, 186. (2022).
162. F. Seidi, C. Deng, Y. Zhong, Y. Liu, Y. Huang, C. Li, and H. Xiao, *Small* 17, 2102453. (2021).
163. R. Puybaret, G. Patriarche, M.B. Jordan, S. Sundaram, Y. El Gmili, J.P. Salvestrini, P.L. Voss, W.A. De Heer, C. Berger, and A. Ougazzaden, *Appl. Phys. Lett.* 108, 103105. (2016).
164. M. Liao, H. Liu, X. Wang, X. Hu, Y. Huang, X. Liu, K. Brennan, J. Mecha, M. Nirmalan, and J.R. Lu, *Curr. Opin. Colloid Interface Sci.* 52, 101417. (2021).
165. F. De Maio, V. Palmieri, G. Babini, A. Augello, I. Palucci, G. Perini, A. Salustri, P. Spilman, M. De Spirito, M. Sanguinetti, and G. Delogu, *Isienc* 24, 102788. (2021).
166. L. Huang, S. Xu, Z. Wang, K. Xue, J. Su, Y. Song, S. Chen, C. Zhu, B.Z. Tang, and R. Ye, *ACS Nano* 14, 12045. (2020).
167. S. Pandit, S. Rahimi, A. Derouiche, A. Boulaoued, and I. Mijakovic, *Sci. Rep.* 11, 1. (2021).
168. W. Chen, R.V. Salvatierra, M. Ren, J. Chen, M.G. Stanford, and J.M. Tour, *Adv. Mater.* 32, 1. (2020).
169. J.Q. Huang, T.Z. Zhuang, Q. Zhang, H.J. Eng, C.M. Chen, and F. Wei, *ACS Nano* 9, 3002. (2015).

170. E. Alhajji, W. Wang, W. Zhang, and H.N. Alshareef, *ACS Appl. Mater. Interfaces*. 12, 18833. (2020).
171. K. Jayaramulu, M. Horn, A. Schneemann, H. Saini, A. Bakandritsos, V. Ranc, M. Petr, V. Stavila, C. Narayana, B. Scheibe, S. Kment, M. Otyepka, N. Motta, D. Dubal, R. Zboril, and R. Fischer, *Adv. Mater.* 33, 2004560. (2021).
172. A.P. Gaur, W. Xiang, A. Nepal, J.P. Wright, P. Chen, T. Nagaraja, S. Sigdel, B. LaCroix, C.M. Sorensen, and S.R. Das, *ACS Appl. Energy Mater.* 4, 7632. (2021).
173. Y. Yun, K.R. Nandanapalli, J.H. Choi, W. Son, C. Choi, and S. Lee, *Nano Energy* 78, 105356. (2010).
174. W. Kong, H. Kum, S.H. Bae, J. Shim, H. Kim, L. Kong, Y. Meng, K. Wang, C. Kim, and J. Kim, *Nat. Nanotechnol.* 14, 927. (2019).
175. FGTR Graphene 1.0. Momodesign <https://en.momodesign.com/products/fgtr-graphene-1-0> (2016).
176. T. Cui, S. Mukherjee, P.M. Sudeep, G. Colas, F. Najafi, J. Tam, P.M. Ajayan, C.V. Singh, Y. Sun, and T. Filleter, *Nat. Mater.* 19, 405. (2020).
177. S. Bhattacharjee, R. Joshi, A.A. Chughtai, and C.R. Macintyre, *Adv. Mater. Interfaces* 6, 1900622. (2019).
178. G-Series. inov-8 <https://www.inov-8.com/us/g-series> (2018).
179. Featuring graphene technology. HEAD <https://www.head.com/us-US/sports/ski/technology/graphene/> (2019).
180. Reebok Thermowarm+Graphene Apparel Collection <https://news.reebok.com/global/latest-news/all/reebok-introduces-thermowarm-graphene-apparel-collection/s/094fd6e8-d17e-4ffe-b827-05b64a14356c> (2021).
181. Zolo Liberty Total-Wireless Earphones https://www.amazon.com/dp/B075JBP2P7/ref=as_li_ss_tl?&linkCode=sl1&tag=grapheneinfo-20&linkId=d1ec85b08fe9fd58712f30ea9c37386d (2017).
182. Sanitary NAPKINS <https://jewelpads.com> (2019).
183. Appear Inc. Smartphone <https://www.appearhome.com> (2021).
184. Direct Plus <https://www.directa-plus.com> (2020).
185. Richard Mille Watch RM <https://www.richardmille.com/collections/rm-50-03-tourbillon-chronograph-mclaren-fl> (2019).
186. G1 AC Filters <https://g1wonders.com/product/g1-wonders-ac-filter-2> (2021).
187. Dassi Interceptor Graphene Bike <https://www.durasport.com.sg/product/dassi-interceptor-graphene-bike-1-2> (2022).
188. Face Mask <https://g1wonders.com> (2020).
189. Graphene paint <https://www.graphenstone.com> (2014).
190. Biosensor <https://www.biolinscientific.com/qsense/sensors> (2016).
191. Concretene <https://www.nationwideengineering.co.uk/concretene/> (2021).
192. Lyten Graphene enhanced Lithium Sulphur Batteries. [online] lyten.com Available at <https://lyten.com/products/batteries/> (2022).
193. Applied Graphene Materials <https://www.appliedgraphenematerials.com/Application/graphene-additives-for-paints-and-coatings/> (2022).
194. Paragraf™ <https://www.paragraf.com/graphene-electronics/ghs/> (2020).
195. Grapheal <https://www.grapheal.com/testnpass> (2020).
196. INBRAIN Neuro-electronics <https://www.inbrain-neuroelectronics.com/> (2021).
197. Integrated Graphene <https://www.integratedgraphene.com/biosensors> (2021).
198. Versarien <https://www.versarien.com/> (2022).
199. National Highway UK <https://nationalhighways.co.uk/our-roads/yorkshire-and-north-east-news/using-graphene-to-improve-roads/> (2021).
200. SpaceBlue <https://spaceblue.co.uk/> (2021).
201. AEH innovative <https://aehinnovativehydrogel.com/> (2021).
202. 2DM <https://2dmsolutions.com/new-launch-aramid-graphene-helmet-with-the-smart-think/> (2021).

Publisher's Note Springer Nature remains neutral with regard to jurisdictional claims in published maps and institutional affiliations.